Diabetes, Metabolic Syndrome and Obesity

Dovepress
Taylor & Francis Group

Open Access Full Text Article

ORIGINAL RESEARCH

Fu-Fang-Qi-Di-Hua-Yu-Tang Improves Diabetic Macrovascular Disease via PI3K/AKT Pathway Regulation

Shizhao Zhang[1,*], Mei Yan[2,*], Pengpeng Liang[1], Ye Zhang[3], Jiamin Liu[1], Hai Huang[1], Guiyun Li[1], Hongyan Wu[1,2]

[1]Shenzhen Hospital, Shanghai University of Traditional Chinese Medicine, Shenzhen, 518000, People's Republic of China; [2]School of Clinical Medicine, Jiangxi University of Chinese Medicine, Nanchang, 330000, People's Republic of China; [3]Pediatrics (TCM), Shenzhen Maternity and Child Healthcare Hospital Co-Construction Hospital, Shenzhen, 518000, People's Republic of China

*These authors contributed equally to this work

Correspondence: Hongyan Wu, Email wu.hy@163.com

Objective: This study aimed to investigate the active ingredients and mechanisms of Fu-Fang-Qi-Di-Hua-Yu-Tang (FFQD) in alleviating atherosclerosis and insulin resistance in diabetic macrovascular disease (DMD) mice.

Methods: Chemical profiling of FFQD was performed using UPLC-Q-TOF-MS. Apoe-/- mice were injected with streptozotocin and fed a high-fat diet to establish DMD. Groups included control (C57BL/6), model (normal saline), low/medium/high-dose FFQD, and western medicine (atorvastatin + metformin). After 12 weeks, aortic morphology, blood glucose/lipid profiles, inflammatory factors, and PI3K/AKT pathway-related targets were analyzed.

Results: FFQD contained 159 identified components. Treatment significantly reduced aortic plaque area, blood glucose, lipids, and lowered the levels of tumor necrosis factor-α (TNF-α), interleukin-6 (IL-6), interleukin-1β (IL-1β), oxidized low-density lipoprotein (ox-LDL), C-reactive protein (CRP), and monocyte chemoattractant protein-1 (MCP-1). It also reduced nitric oxide synthase 2 (NOS2) level, a marker of macrophage polarization, increased arginase 1 (Arg1) level, regulated macrophage polarization, and improved oxidative stress and inflammatory response. In addition, FFQD activated the receptor for advanced glycation end products (RAGE)/PI3K/AKT/mammalian target of rapamycin (mTOR) pathway in the aorta, inhibited RAGE expression, promoted PI3K, AKT, and mTOR phosphorylation, down-regulated microtubule-associated protein 1A/1B-light chain 3-II/I (LC3 II/I) and nuclear factor κB (NF-κB p65) expression, up-regulated SQSTM1 protein (p62) expression, inhibited excessive autophagy, and reduced vascular endothelial damage caused by long-term high glucose levels. In the liver, FFQD activated the Ras family small molecule G protein (RAP1)/PI3K/AKT/forkhead box protein 01 (FOX01) pathway, inhibited RAP1 expression, promoted PI3K and AKT phosphorylation, suppressed FOX01 expression, and improved insulin resistance.

Conclusion: FFQD may improve insulin resistance, regulate glucose and lipid metabolism, inhibit excessive autophagy, induce macrophage polarization, resist inflammation and oxidative stress, inhibit atherosclerosis, and ultimately improve DMD by activating the RAGE/PI3K/AKT/mTOR and RAP1/PI3K/AKT/FOX01 pathways. Therefore, FFQD may be a promising candidate for DMD treatment.

Keywords: Fu Fang Qi Di Hua Yu Tang, diabetic macrovascular disease, insulin resistance, autophagy, ultra performance liquid chromatography quadrupole time of flight mass spectrometry

Introduction

Diabetes is a common metabolic disease, with 537 million cases (incidence rate of 10.5%) worldwide in 2021, projected to increase to 783 million cases (incidence rate of 12.2%) by 2045.[1] Diabetic macrovascular disease (DMD) is one of the most serious and dangerous complications of diabetes. It primarily affects all major arteries in the body, with atherosclerosis and endothelial damage as its basic manifestations.[2] Studies have shown that the risk of cardiovascular and

Received: 23 February 2025
Accepted: 20 June 2025
Published: 8 July 2025

cerebrovascular diseases in diabetic patients is two to four times higher than in non-diabetic patients,[3] and the mortality rate is twice as high.[4] The treatment of DMD has become a serious medical challenge. Many pathogenic factors are associated with DMD, the most direct of which are disorders of glycolipid metabolism and insulin resistance. The pathogenesis is mainly categorized into metabolic disorders, lipid accumulation, excessive production of reactive oxygen species, formation of advanced glycation end products (AGEs), activation of AGE-RAGE axis receptors, flux of polyols and hexosamines, activation of protein kinase C, and chronic vascular inflammation.[5] Autophagy is an important component of cellular activity that plays a significant role in the development of DMD. In a high-glucose and high-lipid environment, vascular endothelial cells undergo excessive autophagy, leading to morphological and functional damage. This impairs their barrier protection, selective permeability, proliferative repair, and secretory regulation functions, ultimately contributing to atherosclerosis. The phosphoinositide 3-kinase/protein kinase B (PI3K/AKT) signaling pathway is widely present in the human body and is a key factor affecting the development of DMD, with insulin resistance and autophagy being closely related.[5,6]

Fu-fang-qi-di-hua-yu-tang (FFQD) comprises Huang Qi, Sheng Di Huang, Tai Zi Shen, Shan Yao, Jiu Huang Jing, Dan Shen, Ji Nei Jin, Cang Shu, Gui Jian Yu, Yin Yang Huo, Huang Lian, and Gan Jiang. Sheng Di Huang and its active ingredients have the effects of lowering blood sugar, lowering blood fat, lowering blood pressure and protecting vascular endothelium;[7,8] Huang Qi and Jiu Huang Jing can treat diabetic macroangiopathy by lowering blood sugar, lowering blood fat, anti-inflammation and anti-oxidative stress;[9–14] Shan Yao and its active ingredients such as diosgenin have long been confirmed to have the effects of anti-diabetes, anti-hyperlipidemia and other metabolic diseases;[15] Yin Yang Huo has anti-inflammatory and insulin resistance improving effects;[16,17] The other herbs have hypoglycemic, lipid-lowering, anti-inflammatory and hemodynamic improving effects.[18–21] Therefore, FFQD has potential advantages in improving DMD. FFQD as a potential therapeutic drug for DMD, although having been long used in clinical practice, had never been systematically investigated regarding its mechanism of action prior to this study. In this study, in vivo experiments explored whether FFQD resisted insulin resistance and inhibited excessive autophagy through the PI3K/AKT signaling pathway, thereby inhibiting the development of DMD.

Methods

Experimental Animals

Specific pathogen-free C57BL/6 pure male mice and Apoe-/- mice (6–8-week-old) were obtained from Zhuhai Best Biotechnology Co., Ltd. (Zhuhai, China; experimental animal use permit number. SCXK(Yue)2020–0051). The mice were housed under controlled environmental conditions (temperature: 23 ± 2°C, humidity: 40–60%) with a 12-h light/dark cycle.

Materials

The Western Diet (D12079B, protein 17 kcal%, carbohydrate 43 kcal%, fat 41 kcal%, and contains approximately 0.21% cholesterol) was obtained from Research Diets (USA). Streptozotocin (STZ) (S0130) was obtained from Sigma Aldrich (USA). The citrate Buffer (C301549) was obtained from Aladdin (USA). The decoction pieces were purchased from the Chinese Medicine Department of Shenzhen Hospital of Shanghai University of Traditional Chinese Medicine, and all met the standards specified in the 2020 edition of the "Pharmacopoeia of the People's Republic of China." Atorvastatin calcium tablets (2401028) were obtained from Lepu Pharmaceutical Technology Ltd. (China), and metformin hydrochloride tablets (202401216C) were obtained from Beijing Jingfeng Pharmaceutical Group Ltd. (China).

UPLC-Q-TOF-MS

Preparation of the Test Solution

Huang Qi, Tai Zi Shen, Shan Yao, Sheng Di Huang, Jiu Huang Jing, Dan Shen, Ji Nei Jin, Cang Shu, Gui Jian Yu, Yin Yang Huo, Huang Lian, and Gan Jiang were combined with 800 mL of water and soaked for 30 min. The mixture was boiled for 1 h and filtered. Subsequently, 600 mL of water was added to the residue, and the mixture was boiled again for 40 min. The filtered liquids were combined and concentrated to 200 mL. The concentrate was then dried under a vacuum.

The dried extract was ground into powder, and 0.1 g was accurately weighed. Next, the powder was mixed with 10 mL of methanol and ultrasonicated (200 W, 40 kHz) for 30 min. The weight loss was made up with methanol, shaken well, and filtered through a 0.22 μm microporous membrane. The filtrate was then collected for testing.

Chromatography

Column: Waters ACQUITYUPLCBEHC 18 column (150 mm × 4.6 mm, 1.7 μm), using sub-2 μm hybrid particle technology, with high column efficiency (theoretical plate number ≥ 5000) and wide pH tolerance (1–12). Mobile phase: 0.1% formic acid aqueous solution (A)-acetonitrile (B), gradient elution program: 0–10 min, 10%~30% B; 10–20 min, 30%~40% B; 20–25 min, 40%~50% B; 25–35 min, 50%~45% B. Flow rate: 0.8 mL/min (meets recommended flow rate range of UPLC system). Column temperature: 25°C (within recommended operating temperature range of BEHC 18 column). Injection volume: 3 μL (optimized for small volume injection to improve sensitivity and meet trace analysis requirements). This configuration allows multi-component separation by gradient elution, balancing resolution and analytical efficiency.

Mass Spectrum

Electrospray ion source (ESI), positive/negative ion detection mode, by adjusting the polarity of spray voltage (positive ion mode 3.0 kV, negative ion mode 2.5–3.5 kV). Multi-charge ionization, suitable for polar compounds and biomacromolecules analysis. Mass scanning range: m/z 100 −1500, covering small molecules to medium molecular weight compounds. Mass center of gravity mode (centroid mode): for accurate molecular weight determination, improve signal-to-noise ratio by filtering noise signal. Nebulizer flow (N_2): 50 L/h, forming stable charged droplets; Desolvation gas flow (N_2): 600 L/h, heating at 300°C to assist rapid evaporation of solvent, improving ionization efficiency. Ion transport optimization: source temperature: 120°C, maintaining stable evaporation of droplets; capillary voltage: 3.0 kV, accelerating ion transport to mass spectrometry; cone voltage: Sample cone 30 V, extraction cone 4.0 V, equilibrium ion transport efficiency and in-source fragmentation.

In vivo Experiment

FFQD Simmering Method

Huang Qi, Tai Zi Shen, Shan Yao, Sheng Di Huang, Jiu Huang Jing, Dan Shen, Ji Nei Jin, Cang Shu, Gui Jian Yu, Yin Yang Huo, Huang Lian, Gan Jiang were mixed with 10 times the amount of distilled water. The mixture was soaked for 30 min and then boiled twice for 40 min each time. The liquid was filtered and heated to concentrate it to 1 g of raw medicine per 1 mL of liquid. After high-temperature sterilization and cooling, the solution was stored at 4°C. The solution was diluted to the required concentration prior to use.

Model Construction and Drug Intervention

The Apoe-/- mice (n = 50) were fed a Western diet and injected intraperitoneally with STZ to induce the DMD model.[22] C57BL/6 mice (n = 10) were used as the control group. After 1 week of adaptive feeding, the Apoe-/- mice continued on a Western diet, whereas C57BL/6 mice were fed a regular diet. After 4 weeks of feeding, when the mice's weight reached 26–30 g, Apoe-/- mice were injected intraperitoneally with 50 mg/kg of STZ (diluted in 0.1 mol/L citrate buffer, pH 4.5) for 5 consecutive days to establish the DMD model. The C57BL/6 mice were injected intraperitoneally with an equal volume of 0.1 mol/L citrate buffer. After 1 week of continued feeding, mice with random blood glucose levels >16.7 mmol/L were considered to have completed model induction and continued on a Western diet for another 7 weeks to complete the model.[22,23] The Apoe-/- mice were randomly categorized into the model, low-dose FFQD (L-FFQD), medium-dose FFQD (M-FFQD), high-dose FFQD (H-FFQD) (7.785 g/kg/d, 15.57 g/kg/d, 31.14 g/kg/d), and combined medicine (ATOR-MAT) (atorvastatin calcium tablets 2.86 mg/kg/d + metformin tablets 107.14 mg/kg/d) groups (10 mice per group). The dose for the drug groups was based on the clinical dose for a 70 kg adult, with the M-FFQD group representing the clinically equivalent dose. Each group was administered the corresponding dose of the drug solution via gavage, while the control and model groups received an equal volume of physiological saline once daily for 12 consecutive weeks.

Enzyme-Linked Immunosorbent Assay

The levels of total cholesterol (TC), triglycerides (TG), low-density lipoprotein cholesterol (LDL-C), and high-density lipoprotein cholesterol (HDL-C) were measured using the corresponding biochemical kits (A110-1-1, A111-1-1, A112-1-1, and A113-1-1, respectively; Nanjing Jiancheng Bioengineering Institute, China) following the manufacturer's instructions. The levels of serum inflammatory cytokines, including interleukin-6 (IL-6), interleukin-1β (IL-1β), tumor necrosis factor-α (TNF-a), monocyte chemoattractant protein-1 (MCP-1), C-reactive protein (CRP), and oxidized low-density lipoprotein (ox-LDL), were determined using enzyme-linked immunosorbent assay kit (CSB-E04741m, CSB-E04639m, CSB-E08054m, CSB-E07933m, CSB-E07923m, CSB-E07430m, Cusabio, China) following the manufacturer's instructions.

Hematoxylin Eosin (HE) Staining

Wax-embedded aortic tissue samples were sectioned into 3-mm slices. After dewaxing and dehydration, the sections were stained with hematoxylin (AWI0001a, Abiowell, China) solution for 3–6 min and 0.5% eosin solution (AWI0029a, Abiowell, China) for 2–3 min. The sections were then sealed with neutral gum (AWI0238a; Abiowell, China) and photographed using a microscope (BA210T; Motic, China).

Real-Time Quantitative Polymerase Chain Reaction (RT-qPCR)

Total RNA was extracted using TRIzol (15596026, Thermo, US), and the concentration of each group was detected using a microspectrophotometer. RNA was reverse transcribed into cDNA using the Superscript III kit following the manufacturer's instructions. PCR amplification was performed under the following conditions: 95°C pre-denaturation for 10 min; 95°C denaturation for 15s, 60°C annealing extensions for 3 s, 40 cycles; 95°C denaturation for 15s, 60°C extension for 30s, 95°C inactivation. β-actin was used as the internal reference, and the relative expression of target mRNAs was assessed using the $2^{-\Delta\Delta Ct}$ method. Primer sequences are provided in Table 1.

Western Blot (WB)

A 25 mg of tissue section was accurately excised and washed with ice-cold PBS, and 300 uL of RIPA lysis buffer was added. The tissues were placed in a biological sample homogenizer and ground until no tissue blocks remained, lysed on ice for 10 min, and then centrifuged at 4°C and 12000 rpm for 15 min. Next, the supernatant was collected, and protein concentration was quantified using a bicinchoninic acid assay. The protein was then denatured by heating at 100°C for 5 min. After gelation, electrophoresis, and membrane transfer, 5% skim milk was prepared with 1 × PBST, and the polyvinylidene fluoride membrane was immersed and left at room temperature for 90 min. The membrane was then

Table 1 Primer Sequences

Primer	Sequence/5'-3'	Length/BP
RAP1	FGACTCAGAAACACAGCCAGACGA RATCACCTTAATGGCAGTTCCC	80
AKT	FCGCCTGCCCTTCTACAACCAG RGCATGATCTCCTTGGCATCCTC	175
PI3K	FGTCCGTCCTGGAGAACTTGG RTGAGGCGTTTCTGGATTGC	152
mTOR	FGCCCAGGCAGAAAACTTACA RCGCAGGAAAGGCATGACGAA	131
Arg1	FCTCCAAGCCAAAGTCCTTAGAG RAGGAGCTGTCATTAGGGACATC	185
NOS2	FGTTCTCAGCCCAACAATACAAGA RGTGGACGGGTCGATGTCAC	127
RAGE	FAAACTTCTGATTCCCGATGGC RACCGCAGTGTAAAGAGTCCC	85
β-actin	FACATCCGTAAAGACCTCTATGCC RTACTCCTGCTTGCTGATCCAC	223

incubated overnight at 4°C with primary antibodies: LC3-II/I (18725-1-AP, Proteintech, USA), NF-κB p65 (10,745-1-AP, Proteintech, USA) (1:500), RAP1 (10,840-1-AP, Proteintech, USA), PI3K (20584-1-AP, Proteintech, USA), P-PI3K (bs-6417R, Bioss, China), mTOR (#2983, CST, USA) (1:1000), P-mTOR (67778-1-Ig, Proteintech, USA) (1:2000), RAGE (16346-1-AP, Proteintech, USA), P-AKT (66444-1-Ig, Proteintech, USA) (1:3000), P62 (18,420-1-AP, Proteintech, USA), AKT (60203-2-Ig, Proteintech, USA), FOX01 (18,592-1-AP, Proteintech, USA), β-actin (66009-1-Ig, Proteintech, USA), and GAPDH (10494-1-AP, Proteintech, USA) (1:5000) antibodies. After the membrane was washed, a secondary antibody (1:5000) was added and incubated at room temperature for 90 min. The membrane was then washed, exposed, and developed using ECL. Finally, the gray values were analyzed using the Image J software.

Statistical Analysis

The results are expressed as mean ± standard deviation ($\bar{x} \pm s$). One-way analysis of variance (ANOVA) was used to compare multiple groups, with statistical significance set at $P < 0.05$. GraphPad Prism 10.3.1 was used for graphical representation.

Ethical Statement

All experimental procedures strictly adhered to the standards for the management and protection of experimental animals (follow the National Research Council Guide for the Care and Use of Laboratory Animals: Eighth Edition (2011)) and were reviewed and approved by the IACUC of the Experimental Animal Center of Shenzhen People's Hospital, with an approval number of AUP-230220-HH-57301.

Results

Characterization of FFQD Chemical Composition

In total, 159 compounds were identified in FFQD, including phenylpropanoids, flavonoids, alkaloids, saponins, and cyclic terpenes. The main components in Huang Qi were flavonoids and triterpene saponins, such as ononin and astragaloside. Tai Zi Shen contained flavonoids and organic acids, as well as characteristic cyclic peptides like heterophyllin B. Cang Shu exhibited fewer components, with characteristic compounds including atractylenolide III and other lactones. Huang Lian primarily consisted of quaternary ammonium isoquinoline alkaloids, such as berberine and coptisine. Dan Shen featured salvianolic acid and tanshinone. Shan Yao had fewer chemical components, with dioscin as a characteristic component. Sheng Di Huang contained cyclic terpenes, such as catalpol and ajugol. Jiu Huang Jing, Gui Jian Yu, and Yin Yang Huo primarily contained flavonoids, with Epimedium brevicornum having characteristic 8-isopentenyl flavonoid glycosides, such as icariin. Gan Jiang was rich in gingerols, such as 6-gingerol and zingerone. In addition, some bile acid compounds were detected in the formula, which were speculated to originate from Ji Nei Jin, along with other common components such as amino acids and sugars. The total ion spectra of the FFQD are shown in Figure 1, the chemical structures of the characteristic components of the FFQD are shown in Figure 2, and specific assignments and identification details of the components are listed in Supplementary Table 1.

FFQD Ameliorates DMD

FFQD Contributes to Improved Blood Glucose and Body Weight in DMD Mice

The control group had lustrous fur, good mental state, normal activity, normal diet, normal body weight, and stable blood glucose levels. In contrast, after modeling, blood glucose levels in the experimental groups significantly increased compared with the control group. After 4 weeks of drug administration, blood glucose levels in the FFQD and ATOR-MAT groups significantly decreased. After modeling, compared with the control group, the body weights of the other groups increased; however, their fur became dull, and they showed signs of hair loss and skin ulcers. During the drug administration period, the body weight of mice in the control group continued to increase. In the model group, the body weight of mice progressively decreased, and by the end of the treatment period, the mice appeared pale, with dry and sparse fur and lean bodies. In the FFQD and ATOR-MAT groups, body weights initially decreased during the early stage

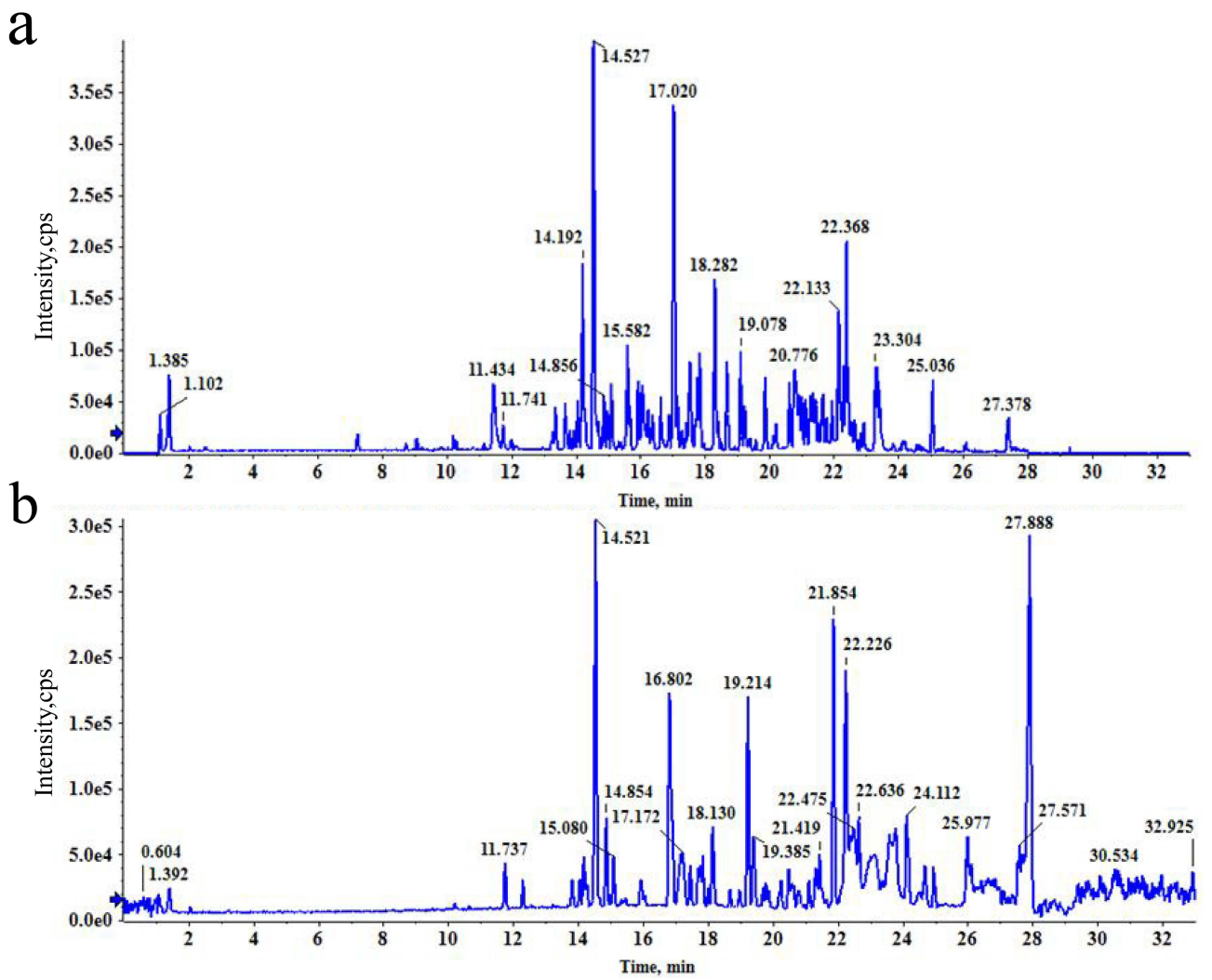

Figure 1 Total ion BPC (Base Peak Chromatogram) spectra of FFQD. (**a**) Negative ions, (**b**) Positive ions. The blue arrow refers to the mass spectrometry intensity fluctuation line.

of drug administration. However, after continuous administration for 8 weeks, their body weights began to increase, and by the end of the drug administration period, their fur was smooth, and their bodies were plump (Figure 3).

FFQD Contributes to the Inhibition of Atherosclerosis in DMD Mice

Aortic plaque deposition and histomorphological changes in the mice were detected using HE staining. No plaque deposition was observed in the aorta of the control group, which maintained an intact endothelial structure with no signs of proliferation or lumen stenosis. In contrast, the model group exhibited substantial plaque deposition, a thickened endothelium, significantly larger plaque areas, and notable lumen stenosis. Compared to the model group, the L-FFQD group exhibited reduced aortic plaque deposition, obvious endothelial thickness, reduced plaque area, and reduced lumen stenosis. M-FFQD further reduced the aortic plaque deposition, the endothelium was thickened, the plaque area was reduced, and the lumen stenosis was reduced. The H-FFQD and ATOR-MAT groups exhibited significantly reduced aortic plaque deposition, reduced endothelial thickening, reduced plaque area, and reduced lumen stenosis (Figure 4).

FFQD Contributes to Improving Lipid Metabolism in DMD Mice

Compared with the control group, serum TC, TG, and LDL-c levels were significantly increased ($P<0.01$), while HDL-c levels were significantly decreased in the model group ($P<0.01$). Compared with the model group, serum TC, TG, and LDL-c levels in the FFQD and ATOR-MAT groups were significantly decreased ($P<0.01$), and HDL-c levels were

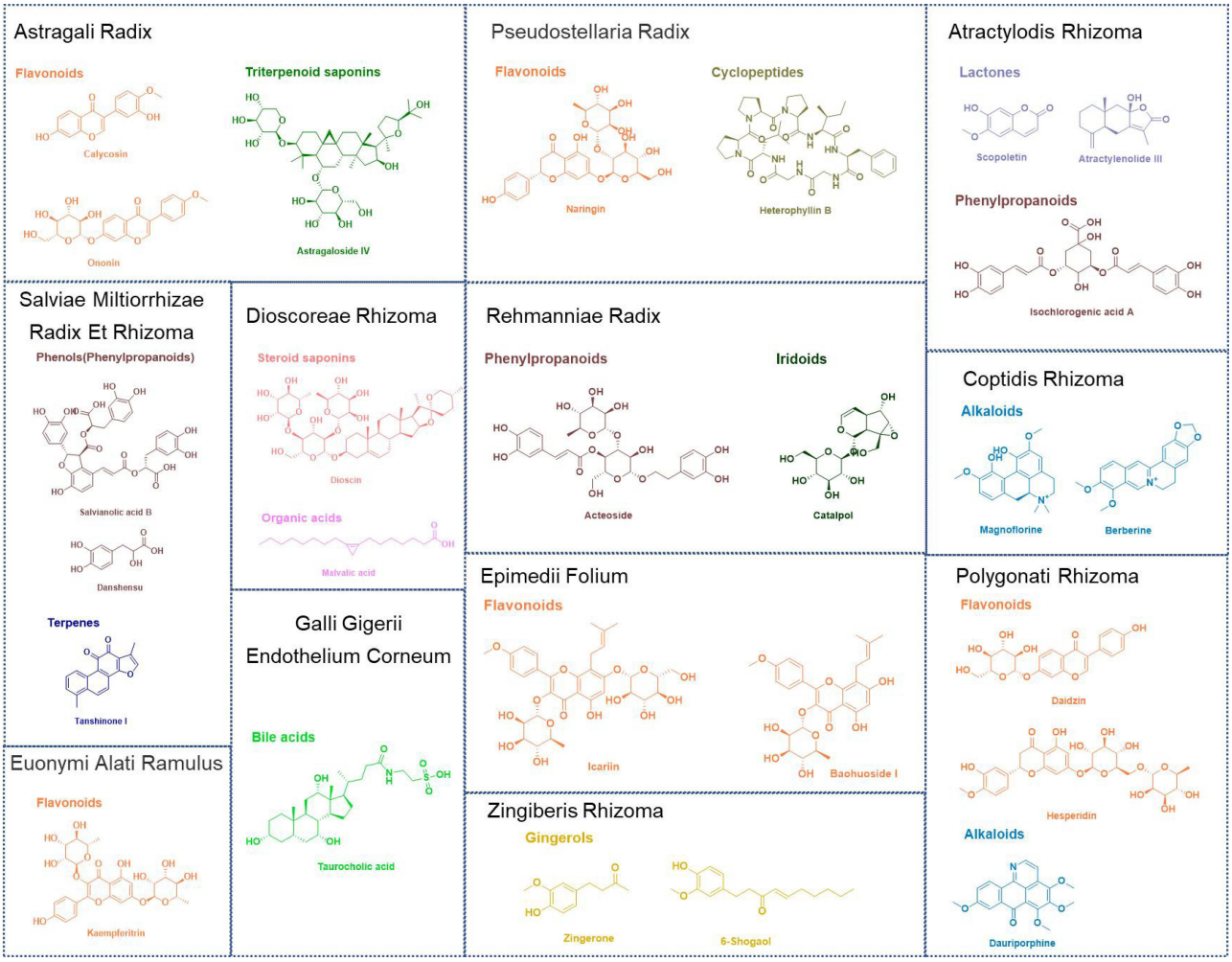

Figure 2 Chemical structures of the characteristic components of FFQD.

increased in the control group ($P<0.01$). Compared with the L-FFQD group, serum TC, TG, and LDL-c levels were significantly decreased (P<0.01), and HDL-c levels were significantly increased in the M-FFQD, H-FFQD, and ATOR-MAT groups ($P<0.01$). Compared with the M-FFQD group, serum TC, TG, and LDL-c levels were significantly decreased ($P<0.01$), and HDL-c levels were increased in the H-FFQD and ATOR-MAT groups ($P<0.01$). Compared with the H-FFQD group, LDL-c levels were significantly higher in the ATOR-MAT group ($P<0.01$), whereas no differences in TC, TG, and HDL-c levels were observed ($P>0.05$) (Figure 5).

FFQD Regulates Insulin Resistance in DMD Mice

Detection of mRNA expression via the RAP1/PI3K/AKT pathway in the liver tissue by RT-qPCR. Compared with the control group, the model group exhibited significant changes in the mRNA expression of PI3K, AKT, mTOR, and RAP1 ($P<0.01$). In the L-FFQD group, RAP1 expression significantly decreased ($P<0.05$), while the changes in PI3K, AKT, and mTOR expression were not significant ($P>0.05$). In the M-FFQD group, PI3K and AKT expression levels significantly increased ($P<0.01$), RAP1 significantly decreased ($P<0.01$), while mTOR expression showed no significant difference ($P>0.05$). Similarly, in the H-FFQD group, PI3K and AKT expression significantly increased ($P<0.01$), RAP1 significantly decreased ($P<0.01$), and mTOR significantly increased ($P<0.05$). In the ATOR-MAT group, PI3K, AKT, and mTOR significantly increased ($P<0.01$), while RAP1 significantly decreased ($P<0.01$). Compared with the L-FFQD group, the mRNA expression of PI3K in the M-FFQD group increased ($P<0.05$), while AKT, mTOR, and RAP1 expression showed no significant differences ($P>0.05$). In the H-FFQD group, the mRNA expression of PI3K and AKT

https://doi.org/10.2147/DMSO.S515521

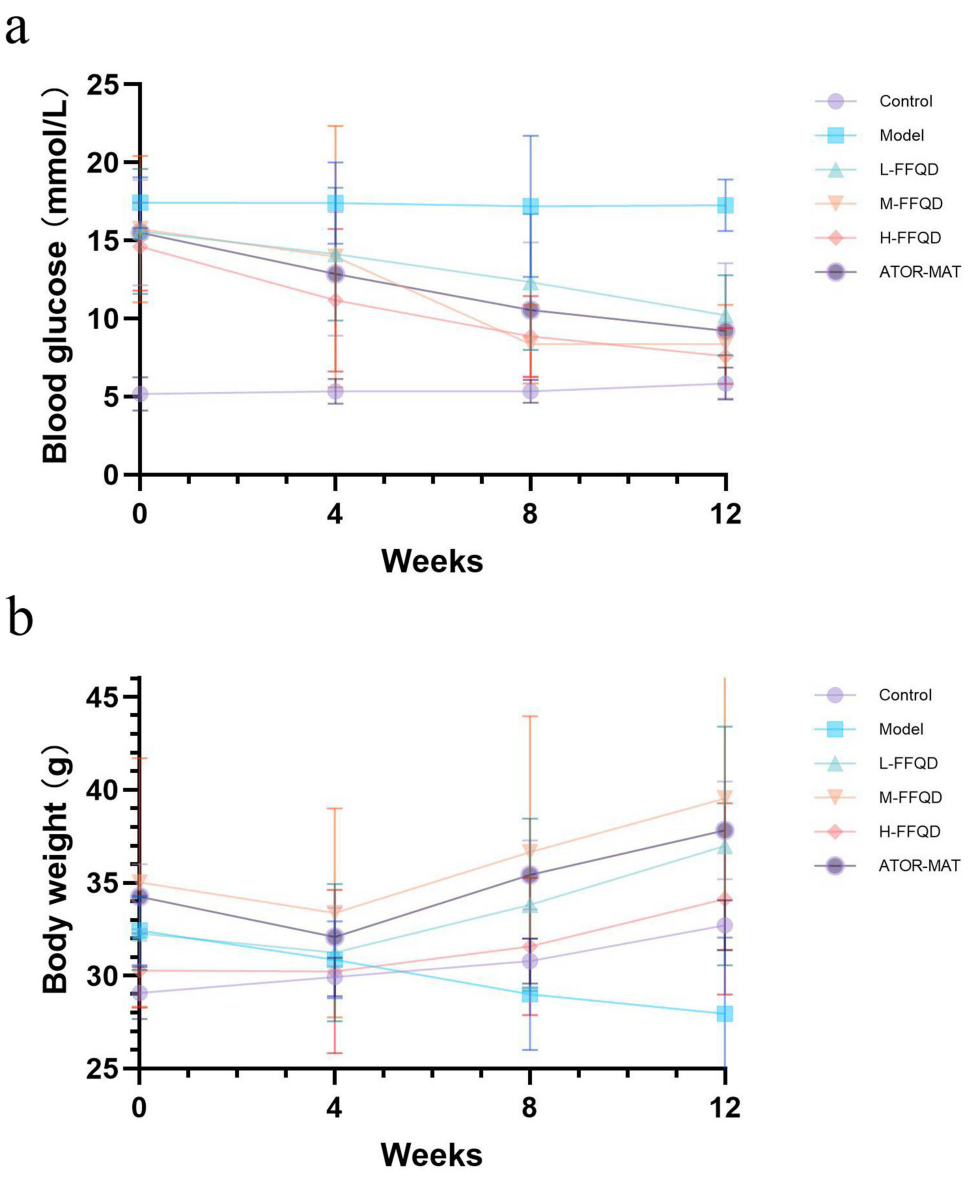

Figure 3 Changes in glucose levels and body weight of mice during drug administration. (**a**) blood glucose; (**b**) body weight.

significantly increased ($P<0.01$), RAP1 significantly decreased ($P<0.01$), and mTOR expression showed no significant differences ($P>0.05$). In the ATOR-MAT group, the mRNA expression of PI3K, AKT, and mTOR significantly increased ($P<0.01$), and RAP1 significantly decreased ($P<0.05$). Compared with the M-FFQD group, the mRNA expression of PI3K in the H-FFQD group significantly increased ($P<0.05$), AKT significantly increased ($P<0.01$), and mTOR and RAP1 expression showed no significant differences ($P>0.05$). In the ATOR-MAT group, the mRNA expression of AKT and mTOR significantly increased ($P<0.01$), while PI3K and RAP1 showed no significant differences ($P>0.05$). Compared with the H-FFQD group, the mRNA expression of AKT in the ATOR-MAT group significantly increased ($P<0.05$), whereas PI3K, mTOR, and RAP1 expression showed no significant differences ($P>0.05$) (Figure 6).

Detection of protein expression levels of the RAP1/PI3K/AKT pathway in the liver tissue by WB Compared with the control group, the model group exhibited significantly reduced P-PI3K/PI3K, P-AKT/AKT, and P-mTOR/mTOR ratios, alongside significantly increased expression of RAP1 and FOX01 ($P<0.01$). Compared with the model group, the M-FFQD group exhibited significantly reduced RAP1 expression ($P<0.01$). The H-FFQD group showed increased ratios of P-PI3K/PI3K and P-mTOR/mTOR ($P<0.05$), significantly increased P-AKT/AKT ratio ($P<0.01$), increased FOX01

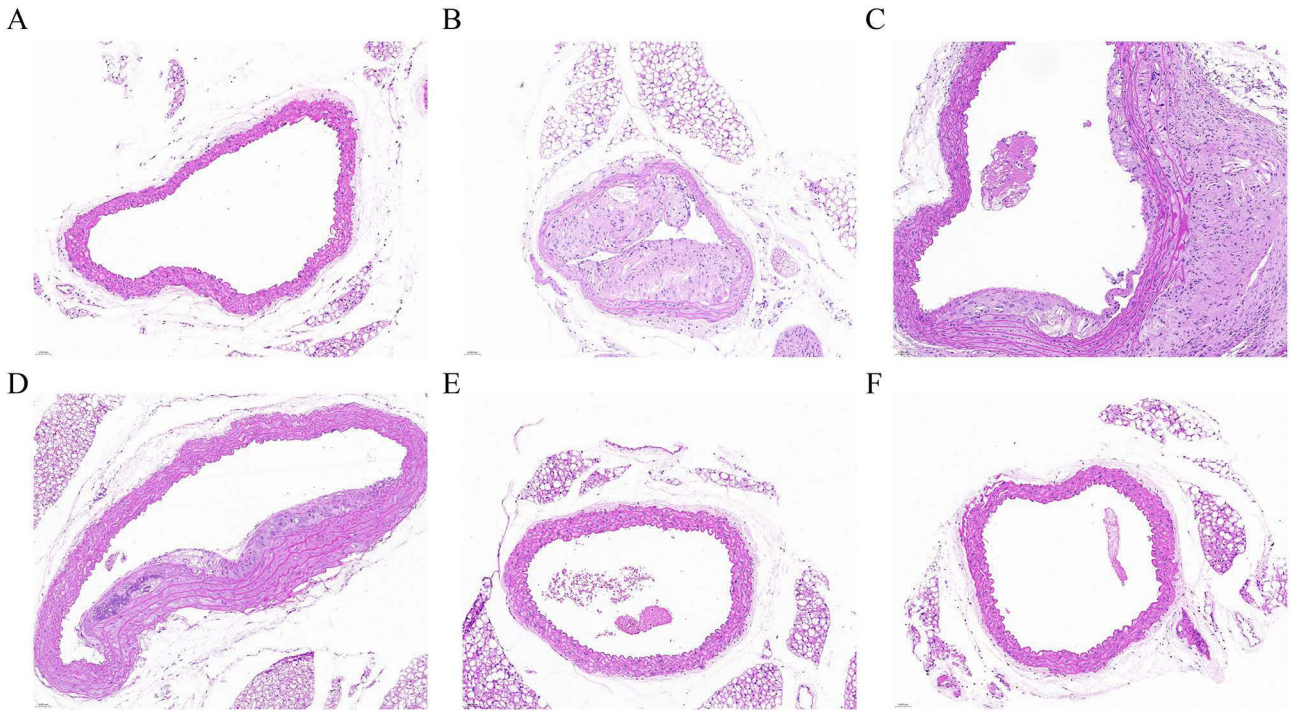

Figure 4 HE staining of aortic tissues in DMD mice (All images were taken under a 20x microscope). (**A**) Control group; (**B**) Model group; (**C**) L-FFQD group; (**D**) M-FFQD group; (**E**) H-FFQD group; (**F**) ATOR-MAT group.

expression ($P<0.05$), and significantly reduced RAP1 expression ($P<0.01$). In the ATOR-MAT group, a significant increase in P-PI3K/PI3K, P-AKT/AKT, and P-mTOR/mTOR ratios was observed, alongside significantly reduced expression of RAP1 and FOX01 ($P<0.01$) (Figure 7).

FFQD Contributes to Alleviating Vascular Inflammation and Oxidative Stress in DMD Mice

Serum levels of IL-6, IL-1β, ox-LDL, CRP, TNF-α, and MCP-1 were significantly increased in the model group compared with the control group ($P<0.01$). Compared with the model group, the levels of IL-6, IL-1β, ox-LDL, CRP, TNF-α, and MCP-1 were significantly decreased in the FFQD and ATOR-MAT groups ($P<0.01$). Compared with the L-FFQD group, the levels of IL-6, IL-1β, ox-LDL, CRP, TNF-α, and MCP-1 were significant in the M-FFQD, H-FFQD, and ATOR-MAT groups ($P<0.01$). Compared with the M-FFQD group, the levels of IL-6, IL-1β, ox-LDL, CRP, TNF-α, and MCP-1 were significantly decreased in the H-FFQD and ATOR-MAT groups ($P<0.01$). Compared with the H-FFQD group, the level of TNF-α was significantly decreased in the ATOR-MAT group ($P<0.01$), whereas no significant differences were observed in the levels of IL-6, IL-1β, ox-LDL, CRP, and MCP-1 ($P>0.05$) (Figure 8).

The expression levels of the aortas macrophage polarization markers recombinant human arginase 1 (Arg1) and nitric oxide synthase 2 (NOS2) were detected using RT-qPCR. Compared with the control group, the model group exhibited significantly reduced Arg1 mRNA expression and significantly increased NOS2 mRNA expression ($P<0.01$). Compared with the model group, the M-FFQD, H-FFQD, and ATOR-MAT groups showed significantly increased Arg1 mRNA expression ($P<0.01$); the FFQD and ATOR-MAT groups exhibited significantly reduced expression of NOS2 mRNA ($P<0.01$) (Figure 9).

FFQD Inhibits Excessive Autophagy in the Aortas of DMD Mice

Detection of mRNA expression levels of the RAGE/PI3K/AKT/mTOR pathway in aortic tissues by RT-qPCR. Compared with the control group, RAGE mRNA expression in the model group was significantly increased ($P<0.01$), while the expression of PI3K, AKT, and mTOR mRNA was significantly decreased ($P<0.01$). Compared with the model group, the expression of RAGE mRNA in the L-FFQD group was significantly reduced ($P<0.01$), and the expression of PI3K, AKT, and mTOR mRNA was increased ($P<0.05$). In addition, RAGE mRNA expression in the M-FFQD, H-FFQD, and

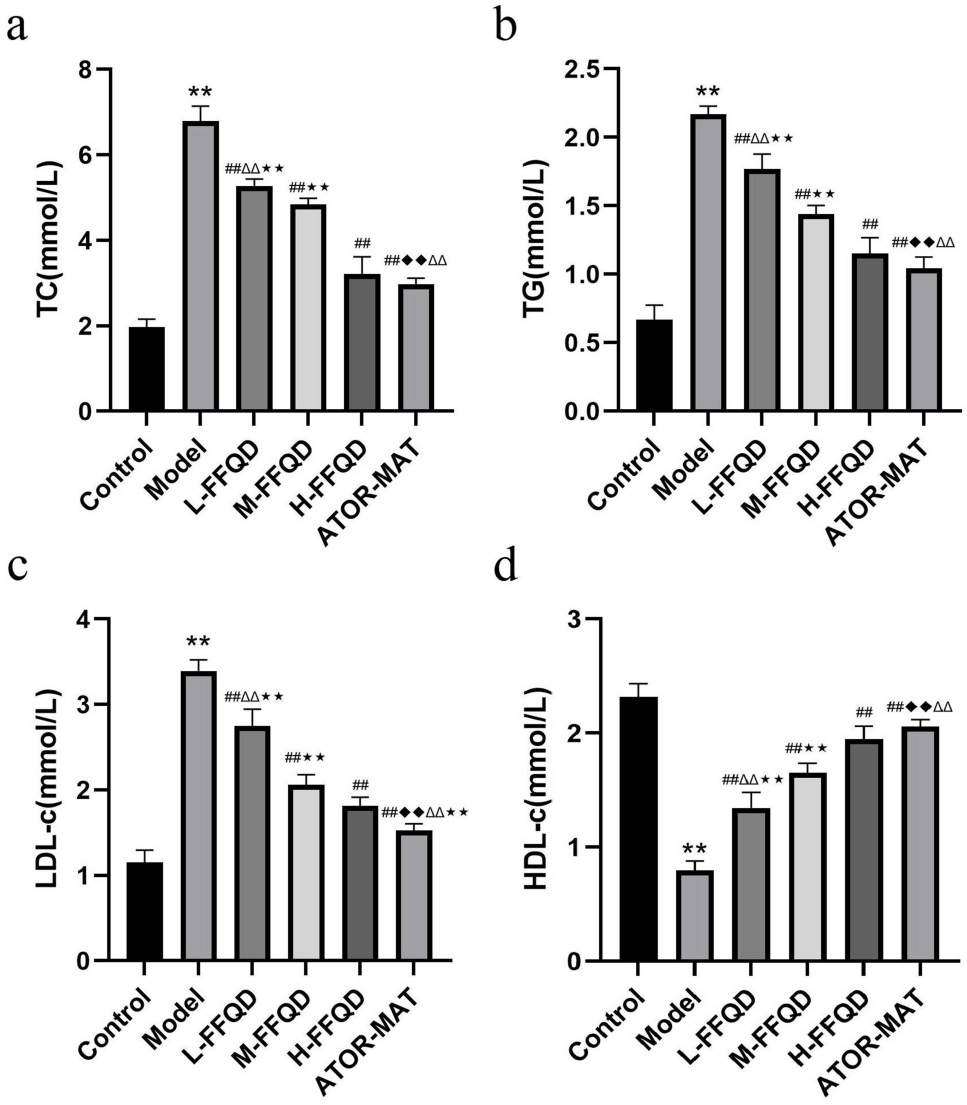

Figure 5 Comparison of serum TC, TG, LDL-c, and HDL-c levels among groups. (**a**) TC levels; (**b**) TG levels; (**c**) LDL-c levels; (**d**) HDL-c levels. Compared with the control (**P<0.01), model ($^{\#\#}P$<0.01), L-FFQD ($^{\blacklozenge\blacklozenge}P$<0.01), M-FFQD ($^{\Delta\Delta}P$<0.01), and H-FFQD ($^{\star\star}P$<0.01) groups, significant differences were observed.

ATOR-MAT groups was significantly reduced (P<0.01), and the expression of PI3K AKT and mTOR mRNA was significantly increased (P<0.01). Significant differences were observed between the L-FFQD and H-FFQD groups (P<0.01) (Figure 10).

Detection of protein expression levels of the RAGE/PI3K/AKT pathway in the aortic tissue by WB. Compared with the control group, the model group showed significantly increased RAGE protein expression (P<0.01) and significantly decreased P-PI3K/PI3K, P-AKT/AKT, and P-mTOR/mTOR (P<0.01). Compared with the model group, the M-FFQD group exhibited decreased RAGE protein expression (P<0.05) and increased P-PI3K/PI3K (P<0.05). The H-FFQD group showed significantly decreased RAGE protein expression (P<0.01), decreased P-AKT/AKT and P-mTOR/mTOR (P<0.05), and significantly increased P-PI3K/PI3K (P<001). Significant differences in P-PI3K/PI3K and RAGE expression were observed between the L-FFQD and H-FFQD groups (P<0.05) (Figure 11a, b, c, d, h). Furthermore, compared with the control group, the model group showed a significant increase in LC3II/I and P65 protein expression (P<0.01), while P62 expression was significantly reduced (P<0.01). Compared with the model group, the L-FFQD group showed increased LC3II/I expression (P<0.05), the M-FFQD group showed decreased LC3II/I and P65 expression (P<0.01), and the H-FFQD group showed increased LC3II/I and P65 expression (P<0.01), whereas P62 expression was significantly

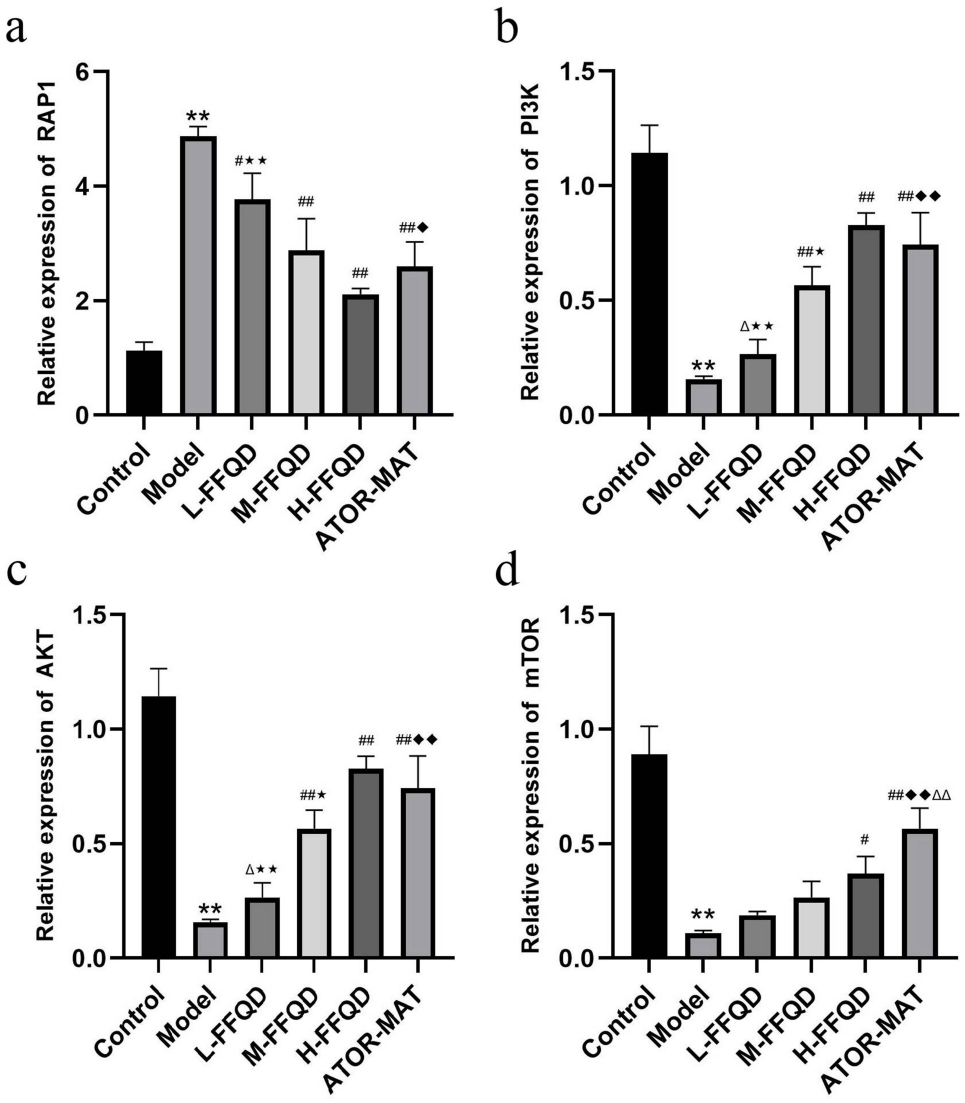

Figure 6 Comparison of mRNA expression via the RAP1/PI3K/AKT pathway among different groups. (**a**) Relative expression of RAP 1; (**b**) Relative expression of PI3K; (**c**) Relative expression of AKT; (**d**) Relative expression of mTOR. Compared with the control ($^{**}P<0.01$), model ($^{\#}P<0.05$, $^{\#\#}P<0.01$), L-FFQD ($^{\blacklozenge}P<0.05$, $^{\blacklozenge\blacklozenge}P<0.01$), M-FFQD ($^{\Delta}P<0.05$, $^{\Delta\Delta}P<0.01$), and H-FFQD ($^{\star}P<0.05$, $^{\star\star}P<0.01$) groups, significant differences were observed.

increased ($P<0.01$). Compared with the L-FFQD group, the H-FFQD group showed a significant decrease in P65 expression ($P<0.01$) and an increase in P62 expression ($P<0.05$) (Figure 11a, e, f, g).

Discussion

DMD, a leading diabetes complication with the highest mortality rate, poses a significant global burden. Autophagy and abnormal glycolipid metabolism are important mechanisms involved in the development of DMD. As a key pathway in insulin resistance and lipid metabolism, the role of PI3K/AKT in the pathogenesis and treatment of DMD remains unexplored. As a traditional Chinese medicine compound used for long-term clinical use, the active ingredients of FFQD and the mechanism for improving DMD were unclear prior to this study. In this study, the chemical components of the FFQD decoction were analyzed, and 159 components were identified, including flavonoids, phenylpropanoids, alkaloids, saponins, iridoids, and other compounds. In addition, FFQD was found to act as an anti-insulin resistance agent, improving blood sugar and lipid levels in DMD mice by regulating the RAP1/PI3K/AKT and RAGE/PI3K/AKT/mTOR pathways, inducing macrophage polarization and reducing inflammatory reactions, inhibiting excessive

https://doi.org/10.2147/DMSO.S515521

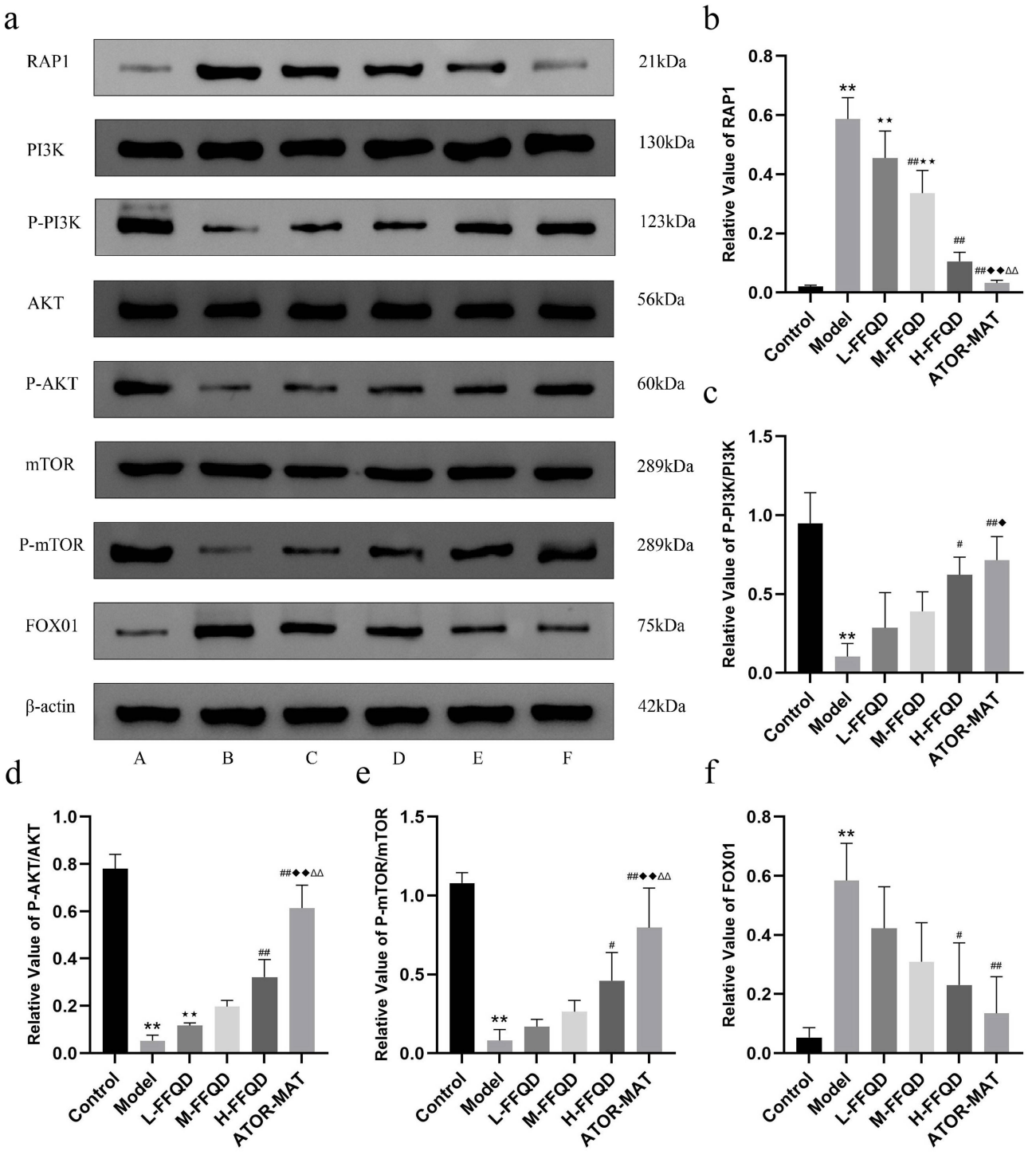

Figure 7 Comparison of protein expression via the RAP1/PI3K/AKT pathway among different groups. (**a**) Electrophoresis of protein expression (A. Control group; B. Model group; C. L-FFQD group; D. M-FFQD group; E. H-FFQD group; F. ATOR-MAT group); (**b**) Relative value of RAP1; (**c**) Relative value of P-PI3K/PI3K; (**d**) Relative value of P-AKT/AKT; (**e**) Relative value of P-mTOR/mTOR; (**f**) Relative value of FOX01. Compared with the control (**$^{**}P$<0.01), model ($^{\#}P$<0.05, $^{\#\#}P$<0.01), L-FFQD ($^{\blacklozenge}P$<0.05, $^{\blacklozenge\blacklozenge}P$<0.01), M-FFQD ($^{\Delta\Delta}P$<0.01), and H-FFQD ($^{\star\star}P$<0.01) groups, significant differences were observed.

autophagy, protecting endothelial function, and inhibiting the development of atherosclerosis, providing a reference for the research, development, and clinical use of DMD therapeutic drugs.

DMD is a gradual process. The most important factor contributing to the onset and development of DMD is a glycolipid metabolism disorder. In a high-sugar and high-lipid environment, insulin-induced liver glycogen synthesis

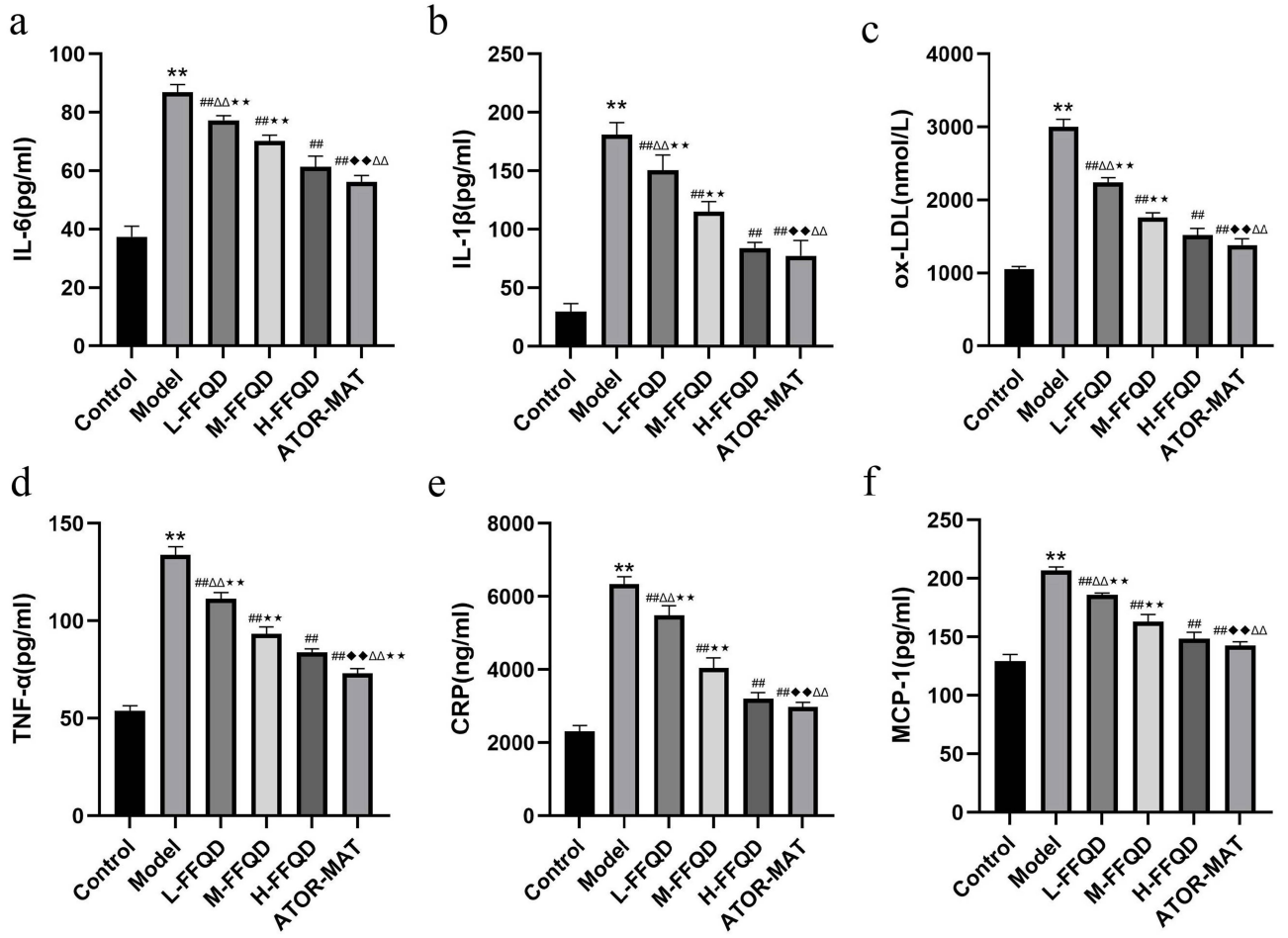

Figure 8 Comparison of serum IL-6, IL-1β, ox-LDL, CRP, TNF-α, and MCP-1 levels among groups. (**a**) IL-6 levels; (**b**) IL-1β levels; (**c**) ox-LDL levels; (**d**) TNF-α levels; (**e**) CRP levels; (**f**) MCP-1 levels. Compared with the control (**P<0.01), model ($^{\#\#}P$<0.01), L-FFQD ($^{\blacklozenge\blacklozenge}P$<0.01), M-FFQD ($^{\Delta\Delta}P$<0.01), and H-FFQD ($^{\star\star}P$<0.01) groups, significant differences were observed.

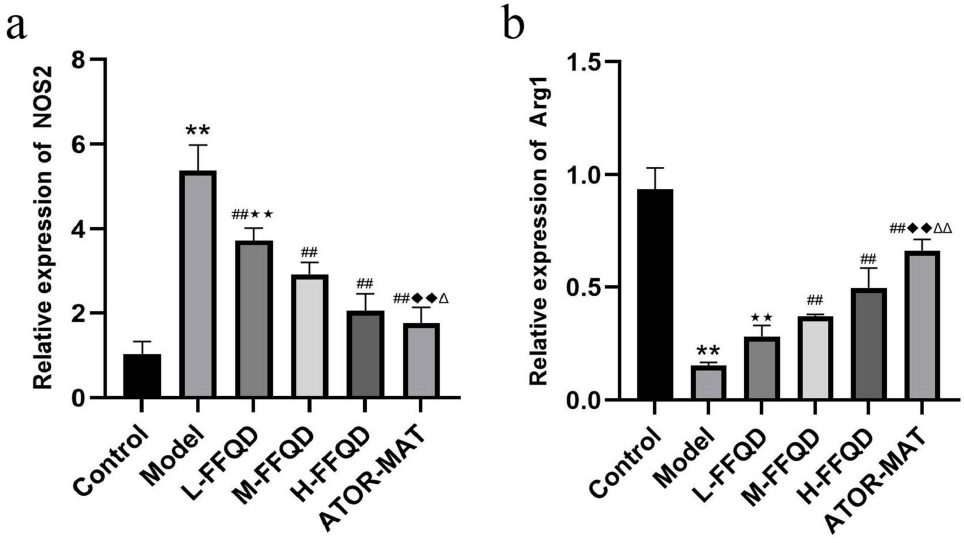

Figure 9 Comparison of mRNA expression of NOS2 and Arg1 among groups. (**a**) Relative expression of NOS2; (**b**) Relative expression of Arg1. Compared with the control (**P<0.01), model ($^{\#\#}P$<0.01), L-FFQD ($^{\blacklozenge\blacklozenge}P$<0.01), M-FFQD ($^{\Delta}P$<0.05, $^{\Delta\Delta}P$<0.01), and H-FFQD ($^{\star\star}P$<0.01) groups, significant differences were observed.

https://doi.org/10.2147/DMSO.S515521

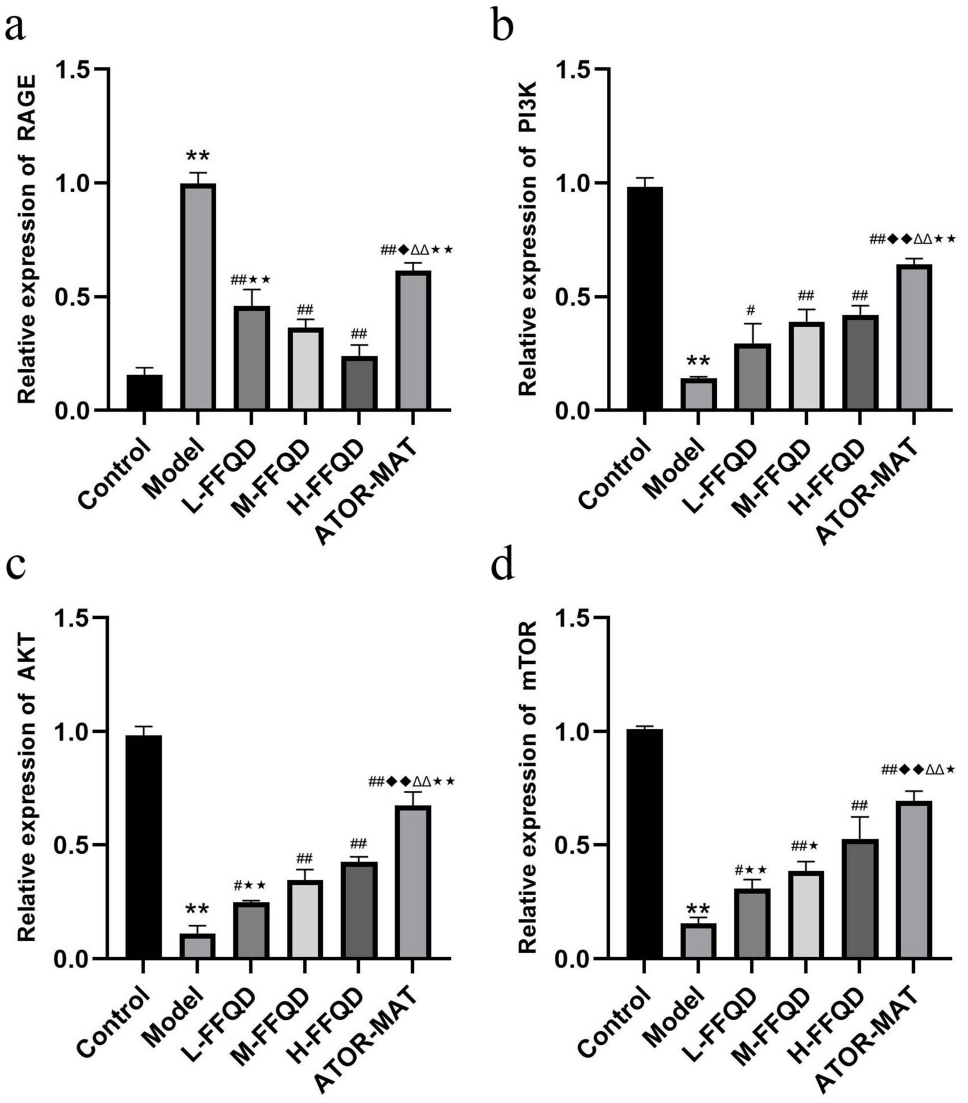

Figure 10 Comparison of mRNA expression via the RAGE/PI3K/AKT/mTOR pathway among different groups. (**a**) Relative expression of RAGE; (**b**) Relative expression of PI3K; (**c**) Relative expression of AKT; (**d**) Relative expression of mTOR. Compared with the control (**P<0.01), model ($^{\#}P$<0.05, $^{\#\#}P$<0.01), L-FFQD ($^{\blacklozenge}P$<0.05, $^{\blacklozenge\blacklozenge}P$<0.01), M-FFQD ($^{\Delta\Delta}P$<0.01), and H-FFQD ($^{\star}P$<0.05, $^{\star\star}P$<0.01) groups, significant differences were observed.

is inhibited, leading to insulin resistance. Moreover, lipid synthesis in the liver tissue is inhibited, and free lipids increase, ultimately leading to an increase in AGEs. AGEs act on the aorta and the circulatory system; they induce the polarization of macrophage M1 phenotype, promoting vascular oxidative stress, inflammation, and foam cell formation. AGEs also bind to RAGE on endothelial cells, stimulating autophagy and damaging endothelial cells, which ultimately leads to atherosclerosis. The PI3K/AKT signaling pathway plays a wide range of key roles in metabolic activities in the human body.[5,6] Most of the extracellular glucose is produced by the kidneys and liver. Only the liver acutely responds to insulin and reduces glucose levels. Glucose is primarily used in the liver for glycogen production and glycogen decomposition.[24] During eating, insulin activates the PI3K/AKT signaling pathway to increase glycogen synthesis and fatty acid synthesis and reduces glycogen production and glycogen decomposition for storage and subsequent utilization by other tissues. FOX01 and mTOR are downstream targets of the PI3K/AKT signaling pathway and are closely associated with glycolipid metabolism.[25,26] FOX proteins, especially FOX01, are the main targets of AKT and affect the energy balance throughout the body.[27] Activated FOX01 and peroxisome proliferation-activated receptor-coactivator 1α (PGC 1α) regulate gene expression and increase glucose production and fatty acid oxidation;[28] they also induce the expression of phosphoenolpyruvate carboxykinase and glucose-6-phosphatase gene, thereby increasing glucose production.[29] After

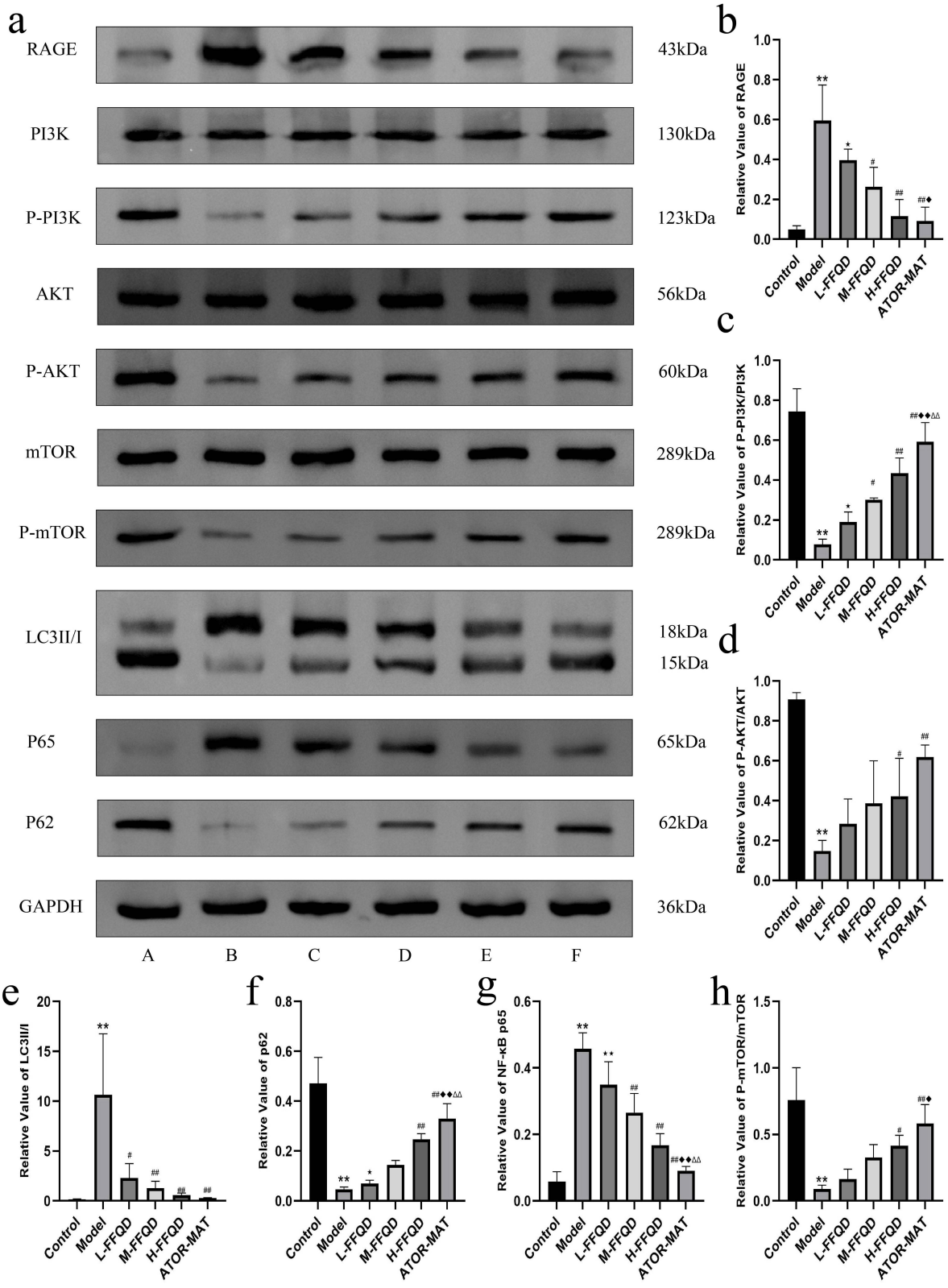

Figure 11 Comparison of protein expression via the RAGE/PI3K/AKT/mTOR pathway among different groups. (**a**) Electrophoresis of protein expression A. Control group; B. Model group; C. L-FFQD group; D. M-FFQD group; E. H-FFQD group; F. ATOR-MAT group); (**b**) Relative value of RAGE; (**c**) Relative value of P-PI3K/PI3K; (**d**) Relative value of P-AKT/AKT; (**e**) Relative value of LC3II/I; (**f**) Relative value of P62; (**g**) Relative value of NF-κB p65; (**h**) Relative value of P-mTOR/mTOR. Compared with the control (**P<0.01), model ($^{\#}P$<0.05, $^{\#\#}P$<0.01), L-FFQD ($^{\blacklozenge}P$<0.05, $^{\blacklozenge\blacklozenge}P$<0.01), M-FFQD ($^{\Delta\Delta}P$<0.01), and H-FFQD ($^{\star}P$<0.05, $^{\star\star}P$<0.01) groups, significant differences were observed.

https://doi.org/10.2147/DMSO.S515521

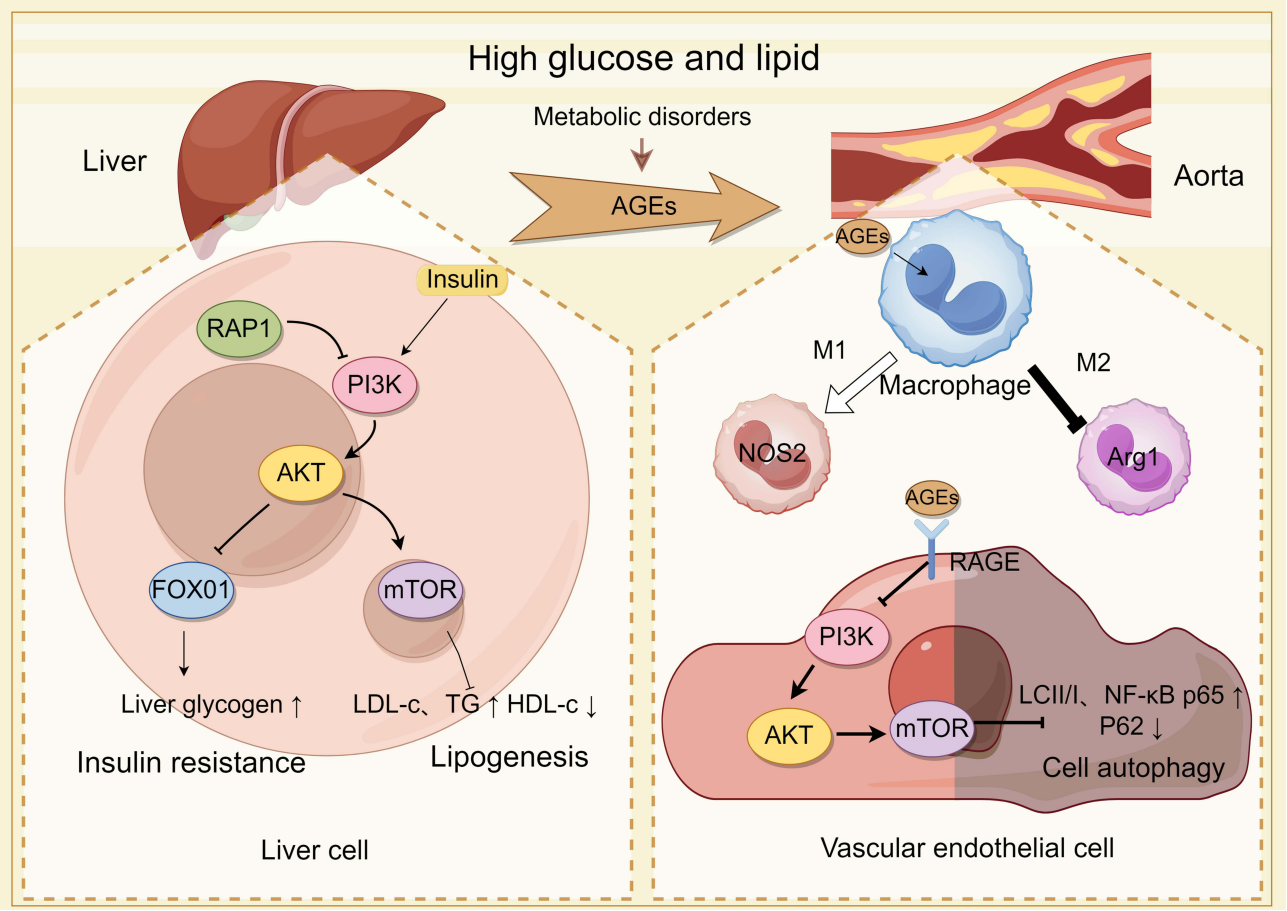

Figure 12 Impact of high glucose and lipid on the PI3K/AKT pathway and DMD. (By Figdraw).

mTOR is activated by AKT, it upregulates the expression of sterol regulatory element-binding proteins, promotes liver lipid synthesis, reduces free fatty acids, and regulates blood lipids.[30] AKT directly inhibits FOX01 and reduces glucose levels while promoting mTOR phosphorylation to increase lipid and protein synthesis[31] and reduce AGE production. Additionally, as an upstream target of PI3K, the role of RAP1 in insulin resistance and lipid metabolism has attracted increasing attention.[32,33] As a member of the GTPhosphate family, RAP1 interacts with multiple pathways to regulate its activity, and the PI3K/AKT signaling pathway is one of its downstream pathways. Studies have shown that, in high-sugar and high-fat environments, RAP1 inhibits the PI3K/AKT pathway, induces insulin resistance, and increases the risk of diabetes and its complications.[34] AGEs produced in glucose and lipid metabolism disorders, such as those in the liver and kidneys, act on blood vessels through the circulatory system. The differentiation of monocytes into macrophages and endothelial cell function is vital for the development of atherosclerosis. Two types of monocytes polarize into macrophages: M1 and M2. Increased polarization of M1 macrophages was observed in AGE-induced monocytes, and an increase in M1-type macrophages would aggravate vascular inflammatory reactions and oxidative stress. In addition, AGEs bind to RAGE on endothelial cell membranes, inhibiting the activation of the PI3K/AKT pathway, reducing mTOR phosphorylation, promoting endothelial cell autophagy, destroying endothelial cells, impairing endothelial function, and exacerbating atherosclerosis (Figure 12).

In this study, compared with the model group, each dose of FFQD effectively improved blood sugar and body weight reduction in DMD mice; significantly reduced serum TC, TG, and LDL-c levels, increased HDL-c levels, and improved glycolipid metabolism were also observed. Inflammatory responses and oxidative stress are important factors in the development of DMD. The results showed that FFQD can effectively reduce the expression level of M1 macrophage marker NOS2, increase the level of M2 macrophage marker Arg1, induce M2 polarization of macrophages, significantly

reduce the levels of IL-6, IL-1β, ox-LDL, CRP, TNF-α, and MCP-1, inhibit inflammatory response and oxidative stress, and reduce vascular damage in DMD mice. Aortic HE staining results also showed that FFQD reduced aortic endothelial damage, atherosclerotic plaque area, and lumen stenosis and inhibited the development of atherosclerosis. Liver tissue PCR and WB results showed that RAP1 mRNA expression increased, whereas the expression of PI3K, AKT, and mTOR mRNA decreased; P-PI3K/PI3K, P-AKT/AKT, and P-mTOR/mTOR expression decreased, and the expression of RAP1 and FOX01 proteins increased in the model group mice. Moreover, the administration of FFQD effectively increased the expression of PI3K, AKT, and mTOR mRNA, decreased the expression of RAP1 mRNA, increased the levels of P-PI3K/PI3K, P-AKT/AKT, and P-mTOR/mTOR, and decreased the expression levels of RAP1 and FOX01 proteins, suggesting that FFQD may improve insulin resistance, promote liver fat synthesis, and reduce free fatty acids and lipoproteins by regulating the RAP1/PI3K/AKT pathway. Aortic PCR and WB results showed that RAGE mRNA expression was significantly increased, and the expression of PI3K, AKT, and mTOR mRNA was significantly decreased in the model group. Moreover, the expression of P-PI3K/PI3K, P-AKT/AKT, P-mTOR/mTOR, and P62 was significantly decreased, and the expression of RAGE, LC3II/I and NF-κ Bp65 was significantly increased. FFQD also effectively reduced RAGE mRNA expression and increased the expression of PI3K, AKT, and mTOR mRNA. These findings suggest that FFQD may regulate the expression of autophagy-related factors LC3II/I, P62, and NF-κB p65 by regulating the RAGE/PI3K/AKT/mTOR pathway, thereby inhibiting excessive autophagy in endothelial cells caused by AGEs, maintaining endothelial integrity, and protecting endothelial function to inhibit atherosclerosis.

Currently, the clinical treatment of DMD involves controlling blood glucose levels combined with antihypertensive medications such as ACEIs and ARBs, statins, PCSK9 inhibitors, antioxidative stress agents, and vasodilators. Antiplatelet drugs may be added for patients at high risk of cardiovascular, cerebrovascular, and peripheral vascular complications.[35] However, long-term use of Western medications cannot fundamentally cure DMD. Moreover, Western drugs primarily alleviate symptoms and may lead to dependency and adverse reactions with prolonged use, increasing both physical and economic burdens on patients and reducing their quality of life. Traditional Chinese medicine (TCM) has been widely applied in treating metabolic and cardiovascular diseases, offering advantages such as low dependency and minimal or no adverse reactions.[36–38] The findings of this study suggest that FFQD may improve metabolic and vascular dysfunction, demonstrating potential therapeutic effects for DMD. This could provide new insights for the clinical management of DMD.

This study had some limitations. The pathogenesis of DMD is complex, and there are additional aspects to explore regarding the mechanisms by which FFQD alleviates DMD. Moreover, the treatment mechanism of FFQD on other diabetic complications represents a valuable direction for future research.

Conclusion

In summary, this study clarified the chemical composition of the FFQD decoction using UPLC-Q-TOF-MS. Through in vivo experiments, it was confirmed that FFQD inhibits insulin resistance and abnormal lipid metabolism via the PI3K/AKT signaling pathway, reduces vascular inflammation and oxidative stress, protects endothelial homeostasis, and improves DMD. These findings provide important insights and a foundation for further exploration of the mechanism by which FFQD improves DMD.

Data Sharing Statement

All data included in this study are available upon request by contact with the corresponding author.

Acknowledgments

We are particularly grateful for the help of the Department of Geriatrics, Shenzhen Hospital, Shanghai University of Traditional Chinese Medicine.

Funding

This study was supported by the Science and Technology Development Project of Guangdong Province (NO.2020A1515010217), the National Prestigious Chinese Medicine Doctor Project ([2022]76), the Scientific research project of Guangdong Provincial Administration of Traditional Chinese Medicine (No. 20222198).

Disclosure

The authors declare that they have no conflicts of interest concerning this article.

References

1. Sun H, Saeedi P, Karuranga S, et al. IDF diabetes atlas: global, regional and country-level diabetes prevalence estimates for 2021 and projections for 2045. *J Diabetes Res Clin Pract*. 2021;183:1019119.
2. Yiwen L, Yanfei L, Shiwei L, et al. Diabetic vascular diseases: molecular mechanisms and therapeutic strategies. *J Signal Transduct Target Ther*. 2023;8:152.
3. Marx N, Federici M, Schütt K, et al. ESC guidelines for the management of cardiovascular disease in patients with diabetes. *J Eur Heart J*. 2023;44 (39):4043–4140.
4. Bragg F, Holmes MV, Iona A, et al. Association between diabetes and cause-specific mortality in rural and urban areas of China. *J JAMA*. 2017;317 (3):280–289. doi:10.1001/jama.2016.19720
5. Xingjun H, Guihua L, Jiao G, et al. The PI3K/AKT pathway in obesity and type 2 diabetes. *J. Int J Biol Sci*. 2018;14(11):1483–1496. doi:10.7150/ijbs.27173
6. Maricedes A-M, Zulema CM. The PI3K/Akt pathway in meta-inflammation. *J Int J Mol Sci*. 2022;23:23.
7. Zhenxian Q, Wei W, Dengqun L, et al. UPLC-Q/TOF-MS-based serum metabolomics reveals hypoglycemic effects of Rehmannia glutinosa, Coptis chinensis and their combination on high-fat-diet-induced diabetes in KK-Ay mice. *J Int J Mol Sci*. 2018;19(12):3984. doi:10.3390/ijms19123984
8. Chao CH, Hsu JL, Chen MF, et al. Anti-hypertensive effects of radix rehmanniae and its active ingredients. *J Nat Prod Res*. 2020;34 (11):1547–1552. doi:10.1080/14786419.2018.1516660
9. Bowei YU, Xiaoqiong P, Jundixia C. Effect of astragalus polysaccharides on glucose and lipid metabolism in diabetic atherosclerosis rats and vascular endothelial protection mechanism. *J J Zhejiang Chin Med Univ*. 2021;45(05):447–453.
10. Fan GE, Wenkai W, Jingtian Z, et al. Astragaloside IV regulates blood lipid and inflammatory factors through NLRP3 inflammasome in early diabetic atherosclerosis rats. *J J Nanjing Univ Tradit Chin Med*. 2021;37(03):383–387.
11. Xiaoqiong P, Zhen HU, Yunxiao L, et al. Effect and mechanism research of astragalus polysaccharides on diabetic atherosclerosis. *J Chin J Clin Pharm*. 2017;26(03):153–157.
12. Xiangduo Z, Yajing X, Bin Q, et al. Effects of polygonatum kingianum Coll. et Hemsl on oxidative stress and expression of Nrf2/HO-1 signaling pathway in diabetes rats with skin lesions. *J Mod Tradit Chin Med Mater Med-World Sci Technol*. 2023;25(09):2959–2966.
13. Mengting T, Lixia L, Huaiying W, et al. Comparison of the polysaccharide components of Radix chinensis, Radix chinensis and its anti-inflammatory and antioxidant effects. *J Chin Tradit Pat Med*. 2023;45(04):1367–1372.
14. Ying L, Ziwei T, Peng T, et al. Adjuvant hypolipidemic effect of Huangjing, black tartary buckwheat, and germinated brown rice in hyperlipidemia mice. *J Pharmacol Clin Chin Mater Med*. 2023;39(09):66–69.
15. Shi-Zhao Z, Peng-Peng L, Ya-Nan F, et al. Therapeutic potential and research progress of diosgenin for lipid metabolism diseases. *J Drug Dev Res*. 2022;83(08):1725–1738. doi:10.1002/ddr.21991
16. Aimei X, Minxiu Y. The mechanism of improving insulin resistance of epimedium in type 2 diabetic rats. *J Chin J Clin Res*. 2012;25(08):731–733.
17. Yongfang S, Qian X, Huiling W, et al. Effects of epimedium on inflammatory factor of type 2 diabetic mellitus rats. *J Proc Clin Med*. 2012;21 (05):359–361.
18. Xu C, You Z, Lin L, et al. Effect of coptis-dried ginger on the dynamic changes of main biomarkers in the cerebrospinal fluid of diabetic rats. *J Cent South Pharm*. 2022;20(04):799–804.
19. Yunhua C, Muxin G, Xulan L, et al. Research progress on the main pharmacological effects and active components of ghost arrow feather and common plants. *J Beijing J Tradit Chin Med*. 2010;29(02):143–147.
20. Chongmin W, Jun L, Haijun J, et al. Research progress of Pseudostellaria heterophylla polysaccharide. *J J Food Saf Qual*. 2021;12(24):9481–9489.
21. Changxing J, Dingyun J, Qingping J, et al. Effect of polysaccharides from Galli Gigerii endothelium corneum on blood lipid, blood glucose and cellular immune function in diabetes mellitus rats with hyperlipidemia. *J Chin J Exp Tradit Med Formul*. 2012;18(20):255–258.
22. Yu J, Liu H, Chen Y, et al. miR-449a disturbs atherosclerotic plaque stability in streptozotocin and high-fat diet-induced diabetic mice by targeting CEACAM1. *J Diabetol Metab Syndr*. 2024;16(1):98. doi:10.1186/s13098-024-01322-y
23. Han WM, Chen XC, Li GR, et al. Acacetin protects against high glucose-induced endothelial cells injury by preserving mitochondrial function via activating Sirt1/Sirt3/AMPK signals. *J Front Pharmacol*. 2021;11:607796. doi:10.3389/fphar.2020.607796
24. Titchenell PM, Quinn WJ, Lu M, et al. Direct hepatocyte insulin signaling is required for lipogenesis but is dispensable for the suppression of glucose production. *J Cell Metab*. 2016;23(6):1154–1166. doi:10.1016/j.cmet.2016.04.022
25. Xiaoya S, Ziqiang C, Yuanyuan M, et al. Resveratrol attenuates dapagliflozin-induced renal gluconeogenesis via activating the PI3K/Akt pathway and suppressing the FoxO1 pathway in type 2 diabetes. *J Food Funct*. 2021;12(3):1207–1218. doi:10.1039/D0FO02387F
26. Qinqin X, Xiaoling Z, Tao L, et al. Exenatide regulates Th17/Treg balance via PI3K/Akt/FoxO1 pathway in db/db mice. *J Mol Med*. 2022;28 (1):144. doi:10.1186/s10020-022-00574-6
27. Peng S, Li W, Hou N, et al. A review of FoxO1-regulated metabolic diseases and related drug discoveries. *J Cells*. 2020;9(1):184. doi:10.3390/cells9010184
28. Li X, Monks B, Ge Q, et al. Akt/PKB regulates hepatic metabolism by directly inhibiting PGC-1-alpha transcription coactivator. *J Nature*. 2007;447(7147):1012–1016. doi:10.1038/nature05861

29. Webb AE, Brunet A. FOXO transcription factors: key regulators of cellular quality control. *J Trends Biochem Sci*. 2014;39(4):159–169. doi:10.1016/j.tibs.2014.02.003
30. Yi J, Zhu J, Wu J, et al. Oncogenic activation of PI3K-AKT-mTOR signaling suppresses ferroptosis via SREBP-mediated lipogenesis. *J Proc Natl Acad Sci USA*. 2020;117(49):31189–31197. doi:10.1073/pnas.2017152117
31. Zini L, Tingting L, Yirui Z. To investigate the regulation of Qiishu capsule on the TCA cycle in diabetic nephropathy rats. *J Chin J Integr Tradit West Nephrol*. 2022;23(04):346–349.
32. Heena A, Brea T, Amesh SK, et al. Rap1 in the context of PCSK9, atherosclerosis, and diabetes. *J Curr Atheroscler Rep*. 2023;25(12):931–937. doi:10.1007/s11883-023-01162-7
33. Yin C, Vidya K, Ramoji K, et al. Decoding telomere protein Rap1: its telomeric and nontelomeric functions and potential implications in diabetic cardiomyopathy. *J Cell Cycle*. 2017;16(19):1765–1773. doi:10.1080/15384101.2017.1371886
34. Kaneko K, Lin HY, Fu Y, et al. Rap1 in the VMH regulates glucose homeostasis. *J JCI Insight*. 2021; 6:e142545.
35. Junbo GE, Jianping WENG, Qiang Z. Chinese expert consensus on the risk assessment and management of panvascular disease in patients with type 2 diabetes mellitus (2022 Edition. *Chin Circul J*. 2022;37(10):974–990.
36. Dai J, Qiu L, Lu Y, et al. Recent advances of traditional Chinese medicine against cardiovascular disease: overview and potential mechanisms. *Front Endocrinol*. 2024;15:1366285. doi:10.3389/fendo.2024.1366285
37. Liu X, Zheng H, Wang F, et al. Developments in the study of Chinese herbal medicine's assessment index and action mechanism for diabetes mellitus. *Animal Model Exp Med*. 2024;7(4):433–443. doi:10.1002/ame2.12455
38. Wei Y, Ding Q, Yeung C, et al. Evidence and potential mechanisms of traditional Chinese medicine for the adjuvant treatment of coronary heart disease in patients with diabetes mellitus: a systematic review and meta-analysis with trial sequential analysis. *J Diabetes Res*. 2022;2022:2545476. doi:10.1155/2022/2545476